J. Fluid Mech. (2009), *vol.* 633, *pp.* 147–158.
doi:10.1017/S0022112009007988 Printed in the United Kingdom

Wall-shear stress patterns of coherent structures in turbulent duct flow

SEBASTIAN GROSSE[1,2]† AND WOLFGANG SCHRÖDER[1]

[1]Institute of Aerodynamics, RWTH Aachen University, D-52062 Aachen, Germany

[2]Laboratory for Aero and Hydrodynamics, Delft University of Technology, 2628 CA Delft, The Netherlands

(Received 5 November 2008 and in revised form 27 April 2009)

The wall-shear stress distribution in turbulent duct flow has been assessed using the micro-pillar shear-stress sensor MPS[3]. The spatial resolution of the sensor line is 10.8 l^+ (viscous units) and the total field of view of 120 l^+ along the spanwise direction allows to capture characteristic dimensions of the wall-shear stress distribution at sufficiently high resolution. The results show the coexistence of low-shear and high-shear regions representing 'footprints' of near-wall coherent structures. The regions of low shear resemble long meandering bands locally interrupted by areas of higher shear stress. Conditional averages of the flow field indicate the existence of nearly streamwise counter-rotating vortices aligned in the streamwise direction. The results further show periods of very strong spanwise wall-shear stress to be related to the occurrence of high streamwise shear regions and momentum transfer towards the wall. These events go along with a spanwise oscillation and a meandering of the low-shear regions.

1. Introduction

The assessment of wall-shear stress and of the velocity field in the viscous sublayer has been the subject of many experimental and numerical studies in the last decades. First, visualizations of the spanwise velocity distribution within the viscous sublayer using hydrogen bubbles as tracer material by Kline *et al.* (1967) or Smith & Metzler (1983) revealed the coexistence of meandering zones of low and high velocity. These zones, low-speed streaks, are closely related to the existence of streamwise vortices, which alternatively transport high-speed fluid towards the wall and low momentum fluid away from it, and which are considered part of the nonlinear vortex interaction system, which transfers wall-normal momentum in a boundary layer and produces turbulence.

Studies, in which the wall-shear stress has been experimentally assessed by near-wall hot wires and wall-mounted hot films (Bakewell & Lumley 1967; Wallace, Eckelmann & Brodkey 1972; Sreenivasan & Antonia 1977; Kreplin & Eckelmann 1979*a*, *b*; Shah & Antonia 1986; Alfredsson *et al.* 1988), have been able to capture quantitative characteristics of the near-wall flow field fortifying the ideas of the structural nature in the viscous sublayer derived from the first flow visualizations. Quite recently, Sheng, Malkiel & Katz (2008) applied the digital holographic particle

† Email address for correspondence: sebastian.grosse@rwth-aachen.de

image velocimetry (PIV) to detect the near-wall velocity field and the associated wall-shear stress distribution in turbulent duct flow.

Apart from these latest results, wall-shear stress studies have mostly been limited to single-point statistics and the distributions of the streamwise and spanwise wall-shear stress components could not be recorded simultaneously or at one single position, such that the two-directional wall-shear stress and its two-dimensional distribution could not be obtained up to now at reasonable spatial resolution. The micro-pillar sensor technique (Grosse & Schröder 2008*a*, 2009*a*) possesses this potential and allows further quantitative insight into near-wall momentum transfer processes. This paper discusses the instantaneous distribution of the streamwise and spanwise wall-shear stress in turbulent duct flow based on wall-shear stress statistics, two-dimensional correlation distributions and conditional averages, and focuses on a further investigation of wave-like patterns of increased spanwise wall-shear stress fluctuations, which have quite recently been discussed by Brücker (2008).

The paper is structured as followed. First, the experimental set-up will briefly be described. In the following, single-point statistics of the wall-shear stress and two-dimensional characteristics of the wall-shear stress distribution revealing the existence of coherent turbulent motion in the proximity of the wall will be reviewed. Consequently, the discussion is focused on the strong spanwise wall-shear stress fluctuations which are considered to be related to sweep events transporting high-speed fluid towards the wall and causing a meandering of low-momentum fluid. A conclusion will wrap up the paper.

2. Experimental set-up

2.1. *The flow facility*

The measurements have been performed in a turbulent duct flow facility with square cross-section. The measurement section possesses a height of $H = 42$ mm. The measurement fluid used is deionized water at constant temperature $T = 20 \pm 0.1^{\circ}$C. The Reynolds number based on the bulk velocity $Re_{H,b} = U_b H/\nu$ is determined from the volume flux V, which can be measured to within 0.3 % accuracy.

The flow enters the duct section through a flow straightener. A tripping device at a contraction ratio of 0.85 is installed 10 D downstream of the straightener and 50 D upstream of the measurement position where the flow can be considered fully developed. The fluid exits the measurement section into an open reservoir and flows through a heat exchanger to maintain constant fluid temperature.

2.2. *The flow field*

The bulk velocity during the wall-shear stress measurements has been set to $0.367\,\mathrm{m\,s^{-1}}$ corresponding to $Re_{H,b} = 15\,400$ or a Reynolds number based on the friction velocity u_τ and the height H of $Re_\tau = 900$. The friction velocity has been determined from the pressure gradient in the measurement section.

The flow field at the centre plane has been investigated using PIV at Reynolds numbers ranging from $Re_{H,b} = 5500$ to $Re_{H,b} = 16\,000$. They showed the lower order statistics of the flow field in the wall-normal plane at the centreline at the higher Reynolds numbers $Re_{H,b}$ to be in good agreement with findings for fully developed two-dimensional channel flow at comparable Reynolds numbers (Kim, Moin & Moser 1987) showing the three-dimensionality of the flow field at the centre plane to reduce to a negligible level.

2.3. *The shear-stress sensor*

The sensor consists of flexible cylinders protruding into the viscous sublayer and bending in reaction to the exerted fluid forces. The optically detected pillar-tip deflection serves as a representative of the local wall-shear stress. A sensor with 12 micro-pillars along the spanwise direction is used in the present study to detect the two-directional wall-shear stress distribution. It is mounted on the duct wall at the centre plane of the measurement section.

A detailed description of the sensor technique can be found in Grosse (2008), Grosse & Schröder (2008*a*,*b*) and Grosse & Schröder (2009*a*). The impact of the sensor structure on the flow field has been thoroughly discussed in Grosse, Schröder & Brücker (2006). Wall-shear stress statistics and turbulent spectra exhibit a constant distribution along sensors oriented in the streamwise direction and the streamwise spatial two-point correlations are in good agreement with data in the literature, which confirms the negligible intrusiveness of the technique in the investigated Reynolds number range and no interaction of sensor structures.

With sensor lengths $L_p \leqslant 5\, l^+$ the structure is fully immersed in the viscous sublayer. The lateral spacing of 0.5 mm corresponds to 10.8 l^+ and the total field of view of approximately 120 l^+ allows the detection of characteristic spanwise length scales of near-wall coherent structures.

Grosse, Soodt & Schröder (2008) showed sensors under the present experimental conditions to exhibit low-pass characteristics with a constant transfer function at frequencies lower than 0.3–0.4 f_0. Possessing eigenfrequencies of $f_0 = 2400 \pm 50$ Hz the sensors in the present study allow to capture the entire spectrum of turbulent frequencies up to the Kolmogorov frequencies of $f_k \approx 200$ Hz at the Reynolds number during the experiments (Hinze 1959; Tennekes & Lumley 1972) at a constant sensor gain and at negligible phase lag.

The sensor is observed using a Schneider Kreuznach macro lens (APO-CPN 4.0-60) mounted on a Photron FASTCAM-X 1024 PCI high-speed camera operated at 1 000 Hz. About 256 000 samples have been recorded such that the total recording time equals 4500 bulk time scales.

2.4. *Taylor's hypothesis and convection velocities*

In the current study only a spanwise sensor line has been applied. Hence, to obtain the streamwise wall-shear stress distribution, Taylor's hypothesis of frozen turbulence (Taylor 1938) has been applied. Although Taylor's hypothesis is only considered to be valid in flow fields with little turbulence intensity, experimental data (Uddin, Perry & Marusic 1997; Dennis & Nickels 2008) and numerical results (Jeon *et al.* 1999; Quadrio & Luchini 2003) showed reasonable agreement between spatial and temporal scales when applying a carefully chosen convection velocity. While the velocity field in the near-wall region is characterized by high fluctuation intensities and high anisotropy, the comparably low diversity of scales in this region and the constancy of their propagation velocity (Jeon *et al.* 1999) might be favourable for the applicability of Taylor's hypothesis. However, it should only be considered an approximation.

The convection velocity, i.e. the mean velocity, at which the near-wall fluid moves along the streamwise direction, has been determined from the temporal auto- and cross-correlation of the wall-shear stress in the streamwise direction with the sensor line being oriented along this direction. The convection velocity of the streamwise fluctuations has been found to be $U_{c,\tau_x} = 0.245\,\mathrm{m\,s^{-1}}$, i.e. 0.667 U_b, 0.545 U_{cl} or 11.53 u_τ. This is in very good agreement with the value of 0.53 U_{cl} for direct

numerical simulation (DNS) channel flow at $Re_\tau = 180$ in Jeon *et al.* (1999). Kim & Hussain (1993) report a constant convection velocity of the streamwise velocity fluctuations at $y^+ \leqslant 5$ at approximately $U_c = 10\ u_\tau$. Kreplin & Eckelmann (1979*b*) report a slightly higher value of 12.1 u_τ. The convection velocity of the spanwise fluctuations U_{c,τ_z} has been found to be approximately 1 % larger.

3. Results

3.1. *Wall-shear stress statistics*

The intensity of the streamwise wall-shear stress fluctuation is $\tau_{x,rms}/\overline{\tau}_x = 0.36$, where $\overline{\tau}_x$ is the mean streamwise wall-shear stress, and it is in good agreement with findings in the literature (Alfredsson *et al.* 1988; Kim *et al.* 1987; Khoo, Chew & Li 1997). The spanwise intensity is $\tau_{z,rms}/\overline{\tau}_x = 0.11$ and is thereby larger than values reported in the literature by Kreplin & Eckelmann (1979*a*) but in the range of values reported by Sirkar & Hanratty (1970). It should be kept in mind that the micro-pillar enables the direct measurement of the spanwise component, whereas the thermal and electrochemical sensors used by Kreplin & Eckelmann (1979*a*) and Sirkar & Hanratty (1970) derive the wall-shear stress from signals of V-shaped probes.

The probability density distributions of the normalized streamwise wall-shear stress fluctuations $\tau_x'/\tau_{x,rms}$ is given in figure 1(*a*). The present results at $Re_{H,b} = 15\,400$ show good agreement with the channel flow findings of Miyagi *et al.* (2000) at similar Reynolds numbers based on the centreline velocity and the channel height ranging from $Re_{H,cl} = 17\,600$ to 35 000, Obi *et al.* (1996) at $Re_{H,cl} = 6600$ and Sheng *et al.* (2008) at $Re_{H,cl} = 100\,000$. The skewness and kurtosis/flatness of the streamwise shear-stress fluctuations are $S_f(\tau_x) = 0.79$ and $F_f(\tau_x) = 3.32$, respectively. The values are slightly smaller than those reported in Grosse & Schröder (2009*b*) since the sensor in the present study has been slightly taller. Note, the values of these higher order moments are known to strongly vary within the viscous sublayer and hence, the length of the pillar sensors influences the derived values (Grosse & Schröder 2008*a*). The probability density function (PDF) of the normalized spanwise wall-shear stress fluctuations $\tau_z'/\tau_{z,rms}$ in figure 1(*b*) exhibits a symmetric behaviour, i.e. $S_f(\tau_z) = -0.01$. The kurtosis is $F_f(\tau_z) = 5.14$ and the PDF appears more peaked than that reported in Sheng *et al.* (2008) but similar to distributions of the spanwise velocity fluctuations in the viscous sublayer of channel flow given in Eckelmann (1974).

The micro-pillar sensor allows to detect both components of the wall-shear stress simultaneously such that joint probability distributions of the streamwise and spanwise fluctuations and the angle of the wall-shear stress vector with respect to the streamwise direction can be computed. The joint probability density distribution (scatter plot) in figure 1(*c*) indicates large streamwise stresses $\tau_x'/\overline{\tau}_x$ to be often accompanied by an increased spanwise component $\tau_z'/\overline{\tau}_x$, which confirms the findings by Sheng *et al.* (2008). The turbulent events related to the occurrence of high spanwise wall-shear stress will be further discussed in § 3.4. Figure 1(*d*) shows the PDF of the wall-shear stress direction and indicates angles of up to 40° with respect to the streamwise direction.

3.2. *Spanwise and streamwise two-point correlations*

Figures 2(*a*) and 2(*b*) show the spanwise distributions of the streamwise and spanwise shear-stress correlations $R_{\tau_x'\tau_x'}(z^+)$ and $R_{\tau_z'\tau_z'}(z^+)$, respectively. The distributions indicate minima of the correlation functions at spanwise locations of 50 z^+ in agreement with correlations of velocity fluctuations $R_{u_x'u_x'}(z^+)$ and $R_{u_z'u_z'}(z^+)$ from

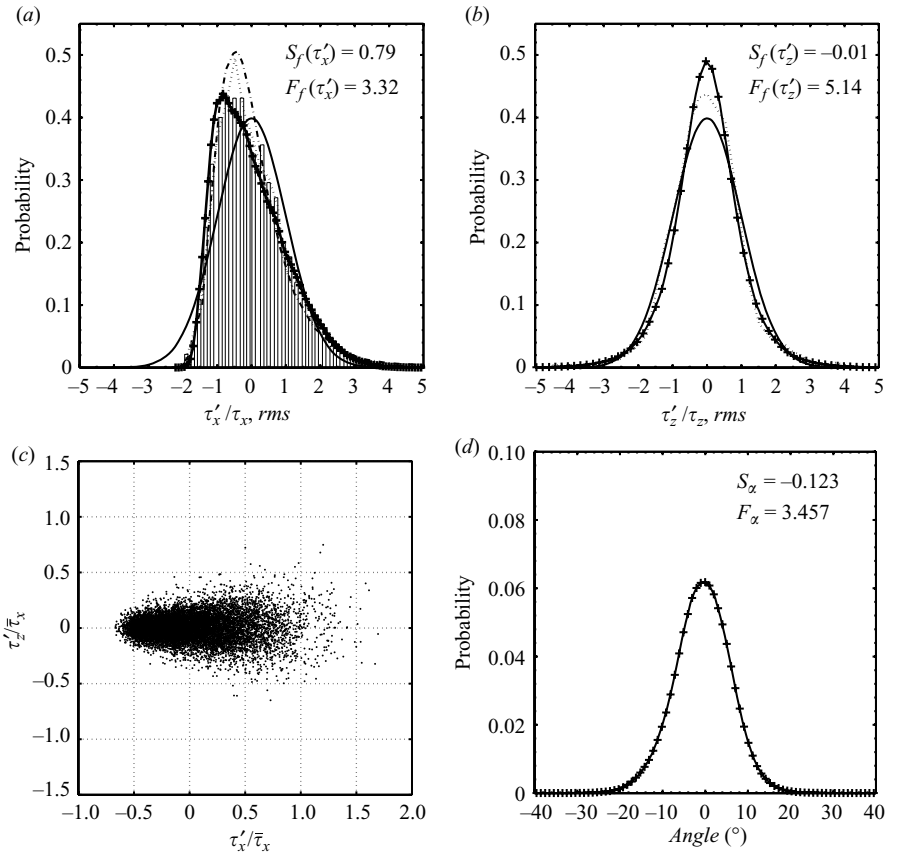

FIGURE 1. (*a*) PDF of the streamwise wall-shear stress fluctuations. $-+-$: present study at $Re_{H,b} = 15\,400$; $-\cdot-$: results reported by Miyagi *et al.* (2000) at $Re_{H,cl} = 17\,600$; bar chart: results reported by Obi *et al.* (1996) at $Re_{H,cl} = 6600$; $\cdots$: results reported in Sheng *et al.* (2008) at $Re_{H,cl} = 100\,000$; —: Gaussian distribution. (*b*) PDF of the spanwise wall-shear stress fluctuations. (*c*) Joint PDF of streamwise and spanwise shear-stress fluctuations. (*d*) PDF of the angle of shear-stress fluctuations.

DNS data (Moser, Kim & Mansour 1999) at $y^+ \approx 5$ and of wall-shear stress DNS data reported by Lyons, Hanratty & McLaughlin (1989). Similar findings for turbulent pipe flow have also been reported in Lee, Eckelman & Hanratty (1974). The DNS data of Jeon *et al.* (1999) indicates slightly higher values for the spanwise distance for $R_{\tau_x'\tau_x'}(z^+)$ and lower values for $R_{\tau_z'\tau_z'}(z^+)$. In the present study, the minima of $R_{\tau_x'\tau_x'}(z^+)$ and $R_{\tau_z'\tau_z'}(z^+)$ are at similar spanwise location, a tendency that was also observed by Lyons *et al.* (1989), who identified the spacing at both distributions at wall distances $y^+ \leqslant 5$ to be rather constant. The spanwise cross-correlation of the shear-stress angle exhibits a similar distribution. However, the negative minimum of the correlation function is less pronounced than $R_{\tau_x'\tau_x'}(z^+)$ and $R_{\tau_z'\tau_z'}(z^+)$.

A comparison of the spatial correlation $R_{\tau_x'\tau_x'}(x^+)$ and $R_{\tau_z'\tau_z'}(x^+)$ along the 12 sensors aligned in the streamwise direction and the correlations from DNS data and those derived from the temporal auto-correlation using Taylor's hypothesis based on the aforementioned convection velocities are given in figures 2(*c*) and 2(*d*), respectively. The findings show very good agreement between the distributions of $R_{\tau_x'\tau_x'}(x^+)$ up to the maximum streamwise spacing of the sensors of approximately 120 x^+ confirming

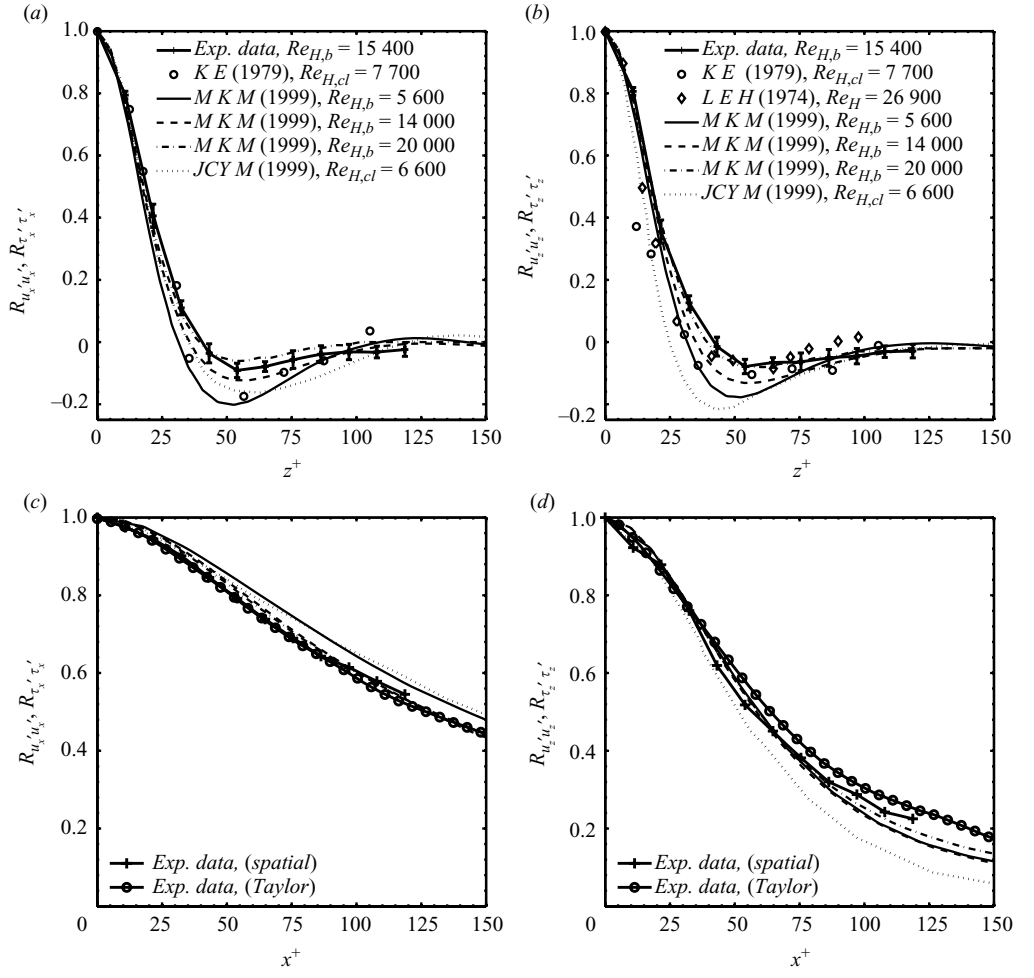

FIGURE 2. (*a*) Spanwise cross-correlation of streamwise shear-stress fluctuations $R_{\tau_{x'}\tau_{x'}}(z^+)$ compared with data of $R_{\tau_{x'}\tau_{x'}}(z^+)$ and $R_{u_{x'}u_{x'}}(z^+)$ in the literature. KE: Kreplin & Eckelmann (1979*b*), MKM: Moser *et al.* (1999), JCYM: Jeon *et al.* (1999) and LEH: Lee, D.Eckelman & Hanratty (1974). (*b*) Spanwise cross-correlation of spanwise shear-stress fluctuations. For symbols see (*a*). Streamwise spatial and temporal (Taylor's hypothesis) cross-correlation of (*c*) streamwise and (*d*) spanwise shear-stress fluctuations at $Re_{H,b} = 15\,400$ compared to data in the literature.

the applicability of Taylor's hypothesis at these streamwise separations, thereby experimentally corroborating the findings from DNS data of Jeon *et al.* (1999) and Quadrio & Luchini (2003). The spatial correlation of the spanwise fluctuations shows good agreement with the DNS at $\Delta x^+ \leqslant 60$–80. At larger distances, the experimental results exhibit larger correlation than the DNS data. In future investigations it is planned to apply sensors over larger streamwise distances to allow for a further investigation of the applicability of Taylor's hypothesis over larger distances.

3.3. *Two-dimensional wall-shear stress distribution*

The two-dimensional cross-correlations of streamwise and spanwise shear-stress fluctuations $R_{\tau_{x'}\tau_{x'}}(x^+, z^+)$ and $R_{\tau_{z'}\tau_{z'}}(x^+, z^+)$, respectively, are shown in figure 3, where the streamwise extension of the distribution has been calculated from the temporal auto-correlation applying Taylor's hypothesis. The streamwise fluctuations correlate

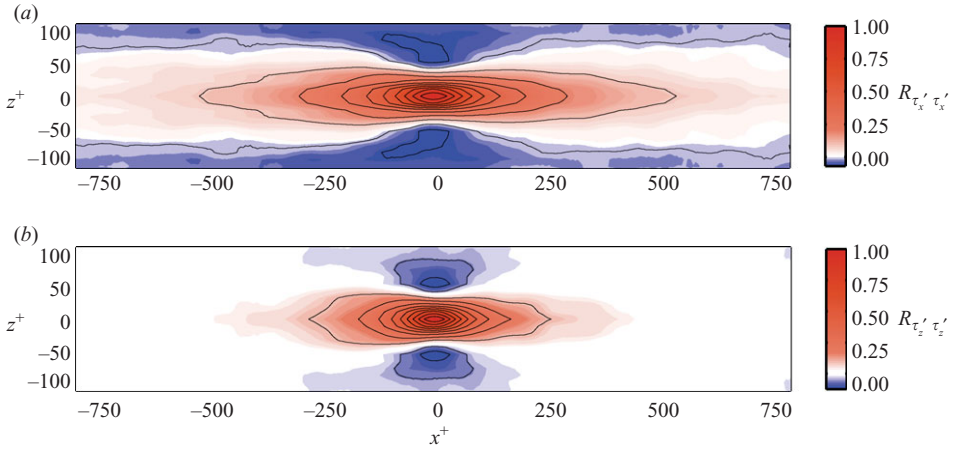

FIGURE 3. Two-dimensional cross-correlation of (*a*) streamwise and (*b*) spanwise shear-stress fluctuations $R_{\tau_x'\tau_x'}(x^+, z^+)$ and $R_{\tau_z'\tau_z'}(x^+, z^+)$, respectively.

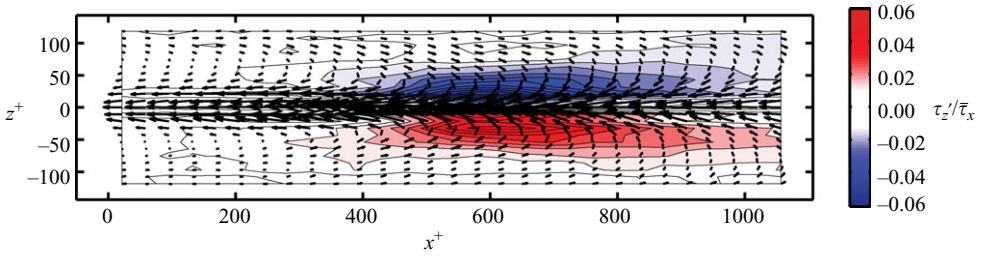

FIGURE 4. Conditional averaged wall-shear stress distribution. The specified event is a local minimum in the streamwise wall-shear stress $\langle \tau'/\overline{\tau}_x \mid \tau_x'/\overline{\tau}_x \leqslant -0.25 \rangle$. Contours indicate the strength of the spanwise wall-shear stress.

positively ($R_{\tau_x'\tau_x'} \geqslant 0.05$–$0.1$) over distances of 500–750 x^+. Two elongated regions of negative correlation aside the central region can be observed indicating the coexistence of elongated streamwise structures with opposite sign. In the case of the spanwise fluctuations the streamwise extent of regions with negative correlation positioned aside the central positive peak is limited to $\pm$50–100 x^+.

The PDF and the visual inspection of instantaneous shear-stress distributions indicates periods of negative wall-shear stress fluctuations to be predominant. To further study structures associated with a local minimum in the wall-shear stress conditional-averaged shear-stress distributions using an event of $\langle \tau'/\overline{\tau}_x \mid \tau_x'/\overline{\tau}_x \leqslant -0.25 \rangle$ have been calculated. The threshold has been chosen similar to that reported by Tomkins & Adrian (2003) for conditional averages of the velocity field at $y^+ \geqslant 21$. The two-directional shear-stress distribution is shown in figure 4. The average shows a central region of negative shear-stress fluctuation and two regions of positive shear-stress fluctuation. The conditional averages show similarities with those reported in Tomkins & Adrian (2003) at a wall distance $y^+ \geqslant 21$. The authors report elliptic counter-rotating vortex patterns in conditional averages of wall-parallel velocity fields which increasingly stretch along the streamwise direction with decreasing wall distance. In the present study, however, closed vortical patterns cannot be observed and the conditional averages rather evidence the existence of extended streamwise shear regions. A possible reason is that at higher regions in

the boundary layer, i.e. $y^+ \geqslant 21$, some of the streamwise vortices already show an inclination with respect to the wall and hence, wall-parallel measurement planes as those by Tomkins & Adrian (2003) cut through the vortical axis, whereas in the wall-shear stress measurements the sensor detects the footprints of the nearly streamwise vortices and consequently, does not cut perpendicular through the vortical axis, which is assumed to be located at approximately $y^+ \geqslant 15$ causing the footprints of the nearly streamwise elongated vortices to appear rather as stretched shear zones aligned in the streamwise direction parallel to the wall.

Results reported by Sheng *et al.* (2008) based on visualizations of the near-wall flow field and the wall-shear stress distribution from holographic recordings of the near wall-region in turbulent duct flow at $Re_{H,cl} = 100\,000$ indicate counter-rotating pairs of streamwise vortices of similar strength and core centres at $3 \leqslant y^+ \leqslant 40$ to cause similar wall-shear stress patterns as those determined from conditional averages in the present study. Unfortunately, the authors do not present statistical averages of the two-dimensional shear-stress field. However, an exemplary wall-shear stress pattern located underneath such a structure (figure 10*a* in Sheng *et al.* 2008) indicates a similar structure as that in the present study, hence, two elongated zones of high streamwise wall-shear stress with a central region of reduced wall-shear stress being approximately 40–50 z^+ wide. The authors further concluded that similar distinct shear structures underneath patterns of multiple (non-counter-rotating) quasi-streamwise vortices in the buffer region could not be detected. Furthermore, they found that the associated wall-shear stress field varied only slightly by $\pm 0.2\,\overline{\tau}_x$, hence, less than the level of the conditional event of $\tau_x'/\overline{\tau}_x \leqslant -0.25$ chosen in the present study.

Note, the symmetry of the conditional average should not be taken as representative. Momentary recordings rather evidence a highly non-symmetric structure of the wall-shear stress distribution, which is characterized by the existence of low-shear regions representing elongated meandering zones of streamwise extensions of order $O(3)\ l^+$ being locally interrupted by high-shear regions (figure 5*c*). Thereby, the findings yield the wall-shear stress distribution to exhibit similar characteristics as the velocity field at slightly higher regions of shear layers. The occurrence of rather local high-shear regions occasionally leads to an intermediate division of the low-shear streak and to a later rejoining at a position further downstream. Similar findings have already been observed by Kline *et al.* (1967) for low-speed streaks from flow visualizations.

Premultiplied spectra of streamwise fluctuations scaled with inner variables (u_τ, ν) peak at frequencies $f^+ = (0.7\text{–}1.2) \times 10^{-2}$, which is in good agreement with earlier findings for turbulent pipe flow at similar Reynolds numbers (Grosse & Schröder 2008*a*) and corresponds to the 1000 l^+ length scale of the near-wall turbulent cycle. However, it should be kept in mind that the calculated spectra are based on single-point statistics and might therefore underestimate the true length of structures along the streamwise direction due to their meandering behaviour. The premultiplied spectra of the spanwise fluctuations scaled with inner variables (u_τ, ν) peak at frequencies $f^+ = (2.0\text{–}2.9) \times 10^{-2}$.

3.4. *Events of increased spanwise wall-shear stress fluctuation*

Quite recently, wave-like patterns of the spanwise wall-shear stress fluctuation have been reported by Brücker (2008). Similar waviness is evident in the two traces of the spanwise wall-shear stress fluctuations exemplarily shown in figure 5(*a*). Figures 5(*b*) and 5(*c*) show the corresponding two-dimensional shear stress distribution with contours indicating the spanwise and streamwise wall-shear stress fluctuations, respectively. Note that the uniform vector lengths in the plots is different along the streamwise and spanwise directions for a better visualization. The position

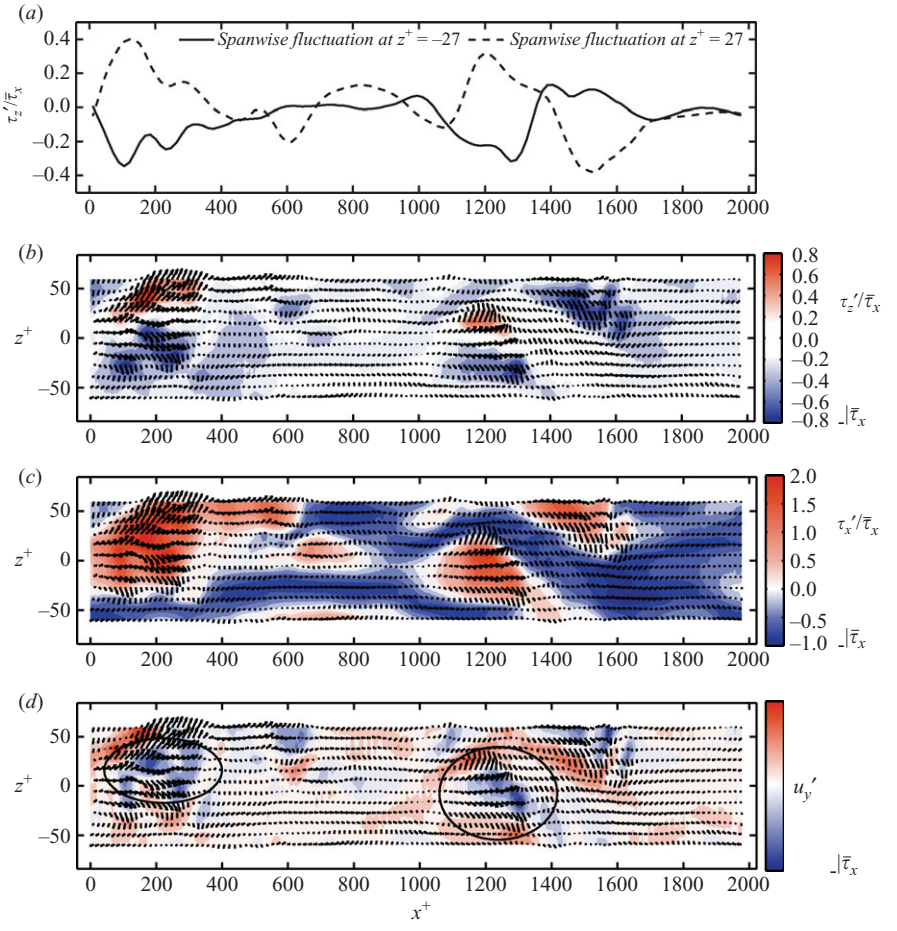

FIGURE 5. (*a*) Spanwise wall-shear stress fluctuations at $\pm 27\ z^+$. (*b*, *c*) Wall-shear stress distributions in an area of $2000 \times 120\ l^+$ in the streamwise and spanwise direction, respectively. Vectors show $\tau'/\overline{\tau}_x$, the contours indicate the (*b*) spanwise and (*c*) streamwise wall-shear stress fluctuations $\tau_z'/\overline{\tau}_x$ and $\tau_x'/\overline{\tau}_x$, respectively. (*d*) Wall-normal velocity fluctuations u_y' calculated from continuity considerations.

of the spanwise shear-stress time traces in figure 5(*a*) is at spanwise positions of approximately $\pm 25\ z^+$, i.e. the distance between the sensor posts is $50\ z^+$. Similar to the findings of Brücker (2008), strong anticorrelation of the fluctuations can be identified, a finding which could already be concluded from the negative values of $R_{\tau_z'\tau_z'}(z^+)$ at $z^+ = 50$ (figure 2*b*). A comparison with figure 5(*c*) shows the positions of the strong anticorrelating spanwise wall-shear stress peaks to be related to the occurrence of high streamwise shear regions, which we relate to sweep events pushing higher speed fluid towards the wall. The co-occurrence of large streamwise and increased spanwise wall-shear stress fluctuations could already be conjectured from the joint PDF in figure 1(*c*). Conditional averaging of the wall-shear stress field associated with the existence of large spanwise fluctuations ($\langle \tau'/\overline{\tau}_x \mid \tau_z'/\overline{\tau}_x \geqslant 0.20 \rangle$) corroborates this finding (figure 6). The exemplary wall-shear stress distributions in figure 5(*c*) and the conditional average indicate the streamwise extension of the structures associated with high spanwise shear to be comparably smaller than that of the low-shear regions discussed in the preceding section. It can be concluded that the

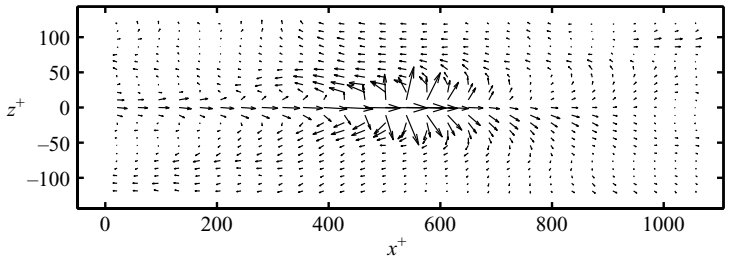

FIGURE 6. Conditional averaged wall-shear stress distribution. The specified event is a local maximum in the spanwise wall-shear stress $\langle \tau'/\overline{\tau}_x \mid \tau_z'/\overline{\tau}_x \geqslant 0.20 \rangle$.

turbulent structure causing the streamwise shear is not simply the elongated sweep region along a streamwise vortex since the associated wall-shear stress pattern can be assumed to be of similar streamwise length as the corresponding low-shear region. Rather quite small-scale sweep events seem to be responsible for the local increase in streamwise and spanwise shear stress.

Similar to the procedure applied by Jiménez & Moin (1991), a rough estimate of the wall-normal velocity (figure 5*d*) has been calculated from continuity considerations assuming the wall-normal velocity to possess a monotonic behaviour within the viscous sublayer. This allows to derive the wall-normal velocity $u_y(L_p)$, where L_p is the wall-distance of the recorded pillar-tips. Furthermore, $-\partial u_y/\partial y = \partial u_x/\partial x + \partial u_z/\partial z$, the latter two terms are derived from the pillar-tip deflection assuming a linear velocity distribution within the sublayer region. A further assumption is that of a constant convection velocity. A comparison of figures 5(*c*) and 5(*d*) indicates regions of high streamwise and spanwise shear to possess negative values of the wall-normal velocity (encircled region), which confirms the idea of sweep fluid approaching the wall. These findings reveal a rather three-dimensional nature of the events, which is thereby in contradiction to the finding of Brücker (2008), who conjectured from the observation of an individual tracer particle trajectory that the wave-like spanwise oscillations are not associated with a change in the wall-normal velocity and rather represent a planar disturbance.

Consequently, the events associated with the existence of high spanwise wall-shear stress are also characterized by high streamwise wall-shear stress values and wall-normal momentum transfer, thereby showing characteristics of sweep motion of high-speed fluid towards the wall. That is, a footprint of this process, which is located in the buffer region of the shear layer, can still be detected in the wall-shear stress distribution. Note, this information can be practically assessed and might therefore be very useful for drag reduction applications (Lee, Kim & Choi 1998; Lee & Kim 2002; Yoshino, Suzuki & Kasagi 2008).

4. Conclusion

The wall-shear stress distribution in turbulent flows evidences the existence of low- and high-shear regions parallely aligned in the streamwise direction. The structure of these regions is characterized by strong spanwise meandering. Typical spanwise extensions of low- and high-shear regions have been confirmed to be of the order of $50\,z^+$.

Conditional averaged patterns with conditional events $\langle \tau'/\overline{\tau}_x \mid \tau_x'/\overline{\tau}_x \leqslant -0.25 \rangle$ further corroborate the existence of low-shear zones caused by near-wall low-momentum structures associated with nearly streamwise vortices. Whether or not these structures group in pairs of counter-rotating vortices can not yet be confirmed from the present findings and further investigations including simultaneous measurements at slightly increased wall distances will be necessary to bring further insight to this question. The statistical shear-stress patterns identified in the present study show very good agreement with data reported in the literature on footprints of near-wall counter-rotating vortices identified from measurements by holographic PIV. However, the present study underlines the general idea of (counter-rotating) nearly streamwise oriented vortices as one of the dominant coherent structures in turbulent shear layers in the extreme vicinity of the wall. Wave-like patterns of large spanwise fluctuations of the wall-shear stress have also been identified and discussed. The temporal development of spanwise fluctuations at spanwise separations of 50 z^+ exhibits a strong anticorrelating behaviour. The events go along with high streamwise shear stress and wall-normal velocities towards the wall in the viscous sublayer thereby revealing a three-dimensional nature of the events. It appears that the additional flux towards the near-wall region is compensated by a spanwise/streamwise fluid spreading causing the high lateral and streamwise fluctuation levels. This behaviour can be observed in instantaneous wall-shear stress distributions and is statistically substantiated by conditional averages of the two-directional wall-shear stress distribution. As such, the events associated with the existence of high spanwise wall-shear stress show typical characteristics of local sweep motion of high-speed fluid originating from higher regions of the shear layer towards the wall.

REFERENCES

Alfredsson, P. H., Johansson, A. V., Haritonidis, J. H. & Eckelmann, H. 1988 The fluctuating all-hear stress and the velocity field in the viscous sublayer. *Phys. Fluids* **31** (5), 1026–1033.

Bakewell, Jr., H. P. & Lumley, J. L. 1967 Viscous sublayer and adjacent wall region in turbulent pipe flow. *Phys. Fluids* **10** (9), 1880–1889.

Brücker, C. 2008 Signature of varicose wave packets in the viscous sublayer. *Phys. Fluids* **20**, 061701.

Dennis, D. J. C. & Nickels, T. B. 2008 On the limitations of Taylor's hypothesis in constructing long structures in a turbulent boundary layer. *J. Fluid Mech.* **614**, 197–206.

Eckelmann, H. 1974 The structure of the viscous sublayer and the adjacent wall region in a turbulent channel flow. *J. Fluid Mech.* **65**, 439–459.

Grosse, S. 2008 Development of the micro-pillar shear-stress sensor MPS^3 for turbulent flows. PhD thesis, Faculty of Mechanical Engineering, RWTH Aachen University, Aachen.

Grosse, S. & Schröder, W. 2008*a* Dynamic wall-shear stress measurements in turbulent pipe flow using the micro-pillar sensor MPS^3. *Intl J. Heat Fluid Flow* **29** (3), 830–840 (Special issue: Fifth International Symposium on Turbulence and Shear Flow Phenomena, TSFP-5, Munich, 2007).

Grosse, S. & Schröder, W. 2008*b* Mean wall-shear stress measurements using the micro-pillar shear-stress sensor MPS^3. *Meas. Sci. Technol.* **19** (1), 015403.

Grosse, S. & Schröder, W. 2009*a* The micro-pillar shear-stress sensor MPS^3. *Sensors* **9** (4), 2222–2251 (Special issue: State-of-the-Art Sensors Technology, Germany).

Grosse, S. & Schröder, W. 2009*b* Two-dimensional visualization of turbulent Wall-Shear stress using micro-pillars. *AIAA J.* **47** (2), 314–321.

Grosse, S., Schröder, W. & Brücker, C. 2006 Nano-Newton drag sensor based on flexible micro-pillars. *Meas. Sci. Technol.* **17** (10), 2689–2697.

Grosse, S., Soodt, T. & Schröder, W. 2008 Dynamic calibration technique for the micro-pillar shear-stress sensor MPS^3. *Meas. Sci. Technol.* **19** (10), 105201.

Hinze, J. O. 1959 *Turbulence,* 1st ed. McGraw–Hill.

Jeon, S., Choi, H., Yoo, J. Y. & Moin, P. 1999 Space-time characteristics of the wall-shear stress fluctuations in a low-Reynolds-number channel flow. *Phys. Fluids* **11** (10), 3084–3094.

Jiménez, J . & Moin, P. 1991 The minimal flow unit in near-wall turbulence. *J. Fluid Mech.* **225**, 213–240.

Khoo, B. C., Chew, Y. T. & Li, G. L. 1997 Effects of imperfect spatial resolution on turbulence measurements in the very near-wall viscous sublayer region. *Exp. Fluids* **22** (4), 327–335.

Kim, J. & Hussain, F. 1993 Propagation velocity of perturbations in turbulent channel flow. *Phys. Fluids* **5** (3), 695–706.

Kim, J., Moin, P. & Moser, R. 1987 Turbulence statistics in fully developed channel flow at low Reynolds number. *J. Fluid Mech.* **177**, 133–166.

Kline, S. J., Reynolds, W. C., Schraub, F. A. & Runstadler, P. W. 1967 The structure of turbulent boundary layers. *J. Fluid Mech.* **30** (4), 741–773.

Kreplin, H.-P. & Eckelmann, H. 1979*a* Behavior of the three fluctuating velocity components in the wall region of a turbulent channel flow. *Phys. Fluids* **22** (7), 1233–1239.

Kreplin, H.-P. & Eckelmann, H. 1979*b* Propagation of perturbations in the viscous sublayer and adjacent wall region. *J. Fluid Mech.* **95** (2), 305–322.

Lee, M. K., Eckelman, L. D. & Hanratty, T. J. 1974 Identification of turbulent wall eddies through the phase relation of the components of the fluctuating velocity gradient. *J. Fluid Mech.* **66** (1), 17–33.

Lee, C. & Kim, J. 2002 Control of the viscous sublayer for drag reduction. *Phys. Fluids* **14** (7), 2523–2529.

Lee, C., Kim, J. & Choi, H. 1998 Suboptimal control of turbulent channel flow for drag reduction. *J. Fluid Mech.* **358**, 245–258.

Lyons, S. L., Hanratty, T. J. & McLaughlin, J. B. 1989 Turbulence-producing eddies in the viscous wall region. *AIChE J.* **35** (12), 1962–1974.

Miyagi, N., Kimura, M., Shoji, H., Saima, A., Ho, C.-M., Tung, S. & Tai, Y.-C. 2000 Statistical analysis on wall shear stress of turbulent boundary layer in a channel flow using micro-shear stress imager. *Intl J. Heat Fluid Flow* **21** (5), 576–581.

Moser, R. D., Kim, J. & Mansour, N. N. 1999 Direct numerical simulation of turbulent channel flow up to $Re_\tau = 590$. *Phys. Fluids* **11**, 943–945.

Obi, S., Inoue, K., Furukawa, T. & Masuda, S 1996 Experimental study on the statistics of wall shear stress in turbulent channel flows. *Intl J. Heat Fluid Flow* **17** (3), 187–192.

Quadrio, M. & Luchini, P. 2003 Integral space-time scales in turbulent wall flows. *Phys. Fluids* **15** (8), 2219–2227.

Shah, D. A. & Antonia, R. A. 1986 Isotropic forms of vorticity and velocity structure function equations in several turbulent shear flows. *Phys. Fluids* **29** (12), 4016–4024.

Sheng, J., Malkiel, E. & Katz, J. 2008 Using digital holographic microscopy for simultaneous measurements of three-dimensional near wall velocity and wall shear stress in a turbulent boundary layer. *Exp. Fluids*.

Sirkar, K. K. & Hanratty, T. J. 1970 The limiting behaviour of the turbulent transverse velocity component close to a wall. *J. Fluid Mech.* **44** (3), 605–614.

Smith, C. R. & Metzler, S. P. 1983 The characteristics of low-speed streaks in the near-wall region of a turbulent boundary layer. *J. Fluid Mech.* **129**, 27–54.

Sreenivasan, K. R. & Antonia, R. A. 1977 Properties of wall-shear stress fluctuations in turbulent duct flow. *J. Appl. Mech.* **44**, 389–395.

Taylor, G. I. 1938 The spectrum of turbulence. *Proc. R. Soc. Lond. Phil. Trans. Ser.* A **164**, 476–490.

Tennekes, H. & Lumley, J. L. 1972 *A First Course in Turbulence*. MIT Press.

Tomkins, C. D. & Adrian, R. J. 2003 Spanwise structure and scale growth in turbulent boundary layers. *J. Fluid Mech.* **490**, 37–74.

Uddin, A. K. M., Perry, A. E. & Marusic, I. 1997 On the validity of Taylor's hypothesis in wall turbulence. *J. Mech. Engng Res. Dev.* **19–20**, 57–66.

Wallace, J. M., Eckelmann, H. & Brodkey, R. S. 1972 The wall region in turbulent shear flow. *J. Fluid Mech.* **54** (1), 39–48.

Yoshino, T., Suzuki, Y. & Kasagi, N. 2008 Drag reduction of turbulence air channel flow with distributed micro sensors and actuators. *J. Fluid Sci. Technol.* **3** (1), 137–148.